

# On the critical signatures of neural activity

Benedetta Mariani,<sup>1,2</sup> Giorgio Nicoletti,<sup>1</sup> Marta Bisio,<sup>2,3</sup>  
Marta Maschietto,<sup>3</sup> Stefano Vassanelli,<sup>2,3</sup> and Samir Suweis<sup>1,2</sup>

<sup>1</sup>*Department of Physics and Astronomy “Galileo Galilei”, University of Padova, Padova, Italy*

<sup>2</sup>*Padova Neuroscience Center, University of Padova, Padova, Italy*

<sup>3</sup>*Department of Biomedical Science, University of Padova, Padova, Italy*

The critical brain hypothesis has emerged as an attractive framework to understand neuronal activity, but it is still widely debated. We show that power-law neuronal avalanches satisfying the crackling-noise relation emerge in a paradigmatic model as a sole consequence of external modulation, which induces an extrinsic mutual information in the system. Using data from multi-electrodes array probes in the rat’s cortex, we find that the spatial correlations display typical features of critical systems and we show that our model, with the addition of intrinsic interactions, reproduces these critical scale-free correlations, coexisting with and disentangled from externally-driven power-law avalanches.

The critical brain hypothesis has been much investigated since scale-free neuronal avalanches were found in 2003 by Beggs and Plenz [1–9]. In their seminal work they showed that, by analyzing Local Field Potentials (LFPs) from cortical slices and cultures on chips, cascades of neuronal activity are power-law distributed in their sizes and lifetimes, with exponents remarkably close to the ones of a critical branching process. Since then, such power-laws have been repeatedly observed in experiments [10–15] suggesting that the brain might be poised near the critical point of a phase transition. However, this hypothesis is still widely debated [16–26], and reconciling the different views and experimental results remains pressing.

On the one hand, many subsequent works showed that the presence of power-law avalanches is not a sufficient condition for criticality, as they might emerge from different mechanisms [18–21]. What is now considered one of the stringest test for criticality is whether avalanche exponents satisfy the crackling-noise relation [27, 28], which is believed to hold exactly only at criticality [29]. Moreover, recent findings [22, 30] suggest that the avalanche exponents found in different experimental settings lay along the scaling line defined by the crackling-noise relation with a seemingly universal exponent  $\delta \approx 1.28$ . However, this relation can be fulfilled even in models of independent spiking units, for a range of choices of the power-law fitting method [24]. Arguably, a more fundamental signature of criticality is the presence of long-range correlations in space [31], which manifest themselves in a correlation length that scales with the system size. Nevertheless, these methods have usually been applied at coarser scales, such as in whole brain data [32, 33], and not in specific cortical areas [34]. When such spatial information is not available, phenomenological renormalization group procedures [35, 36] have been recently proposed.

On the other hand, the debate about the “nature” of the transition is very much open, and thus its hypothetical universality class is poorly understood. In particular, recent works have proposed that the observed transition might be related to a synchronous-asynchronous

one [29, 37–39] or a disorder-induced transition [33], contrarily to the original, simpler hypothesis of a critical branching process. All in all, these results still lack a unifying framework. In this work, we show that signatures of criticality beyond avalanches are present in spatial LFPs, in the form of a spatial correlation length that grows with the system size. Then, we introduce an archetypal framework in which the origin of these different signatures can be disentangled, shedding a light on the underlying mechanisms from which such properties of neural activity emerge. In particular, our work suggests that, whereas avalanches may emerge from extrinsic stochasticity, interactions between neural populations are the fundamental biological mechanism that gives rise to seemingly scale-free correlations.

We measured the population activity in the primary somatosensory cortex of four rats using state of the art spatially-extended multi-electrodes arrays. The cortical activity is recorded through a 256-channels array organized in a  $64 \text{ rows} \times 4 \text{ columns}$  matrix with an inter-electrode distance of  $32 \mu\text{m}$  [41], see Figure 1a. The avalanche statistics is analyzed in LFPs data following standardized pipelines for event detection [10, 13, 41, 42], and we report a full statistical analysis of our dataset in [43]. Briefly, the distribution  $p(s)$  of the avalanches sizes and of the avalanche duration  $p(T)$  are computed and fitted using a corrected maximum likelihood method [41, 43, 44]. We find that both are statistically compatible with the expected power-laws  $P(s) \sim s^{-\tau}$  and  $P(T) \sim T^{-\tau_t}$  as we show in Figure 1b-c. Averaging over four rats, we find an inter-rat variability with average exponents  $\langle \tau \rangle = 1.75 \pm 0.1$  and  $\langle \tau_t \rangle = 2.1 \pm 0.3$  [41]. In Figure 1d we show that the crackling-noise relation [27] holds, by comparing  $\delta_{\text{pred}} = \frac{\tau_t - 1}{\tau - 1}$  with the exponent obtained from  $\langle s(T) \rangle \sim T^{\delta_{\text{fit}}}$ . Averaging over each of our rats, we find  $\langle \delta_{\text{pred}} \rangle = 1.47 \pm 0.18$  and  $\langle \delta_{\text{fit}} \rangle = 1.46 \pm 0.04$ . Further details on the fitting procedure can be found in [43].

We then focus on the spatial correlations of the fluctuations of the measured LFP activity and whether they display any signature of criticality [32, 45]. By studying

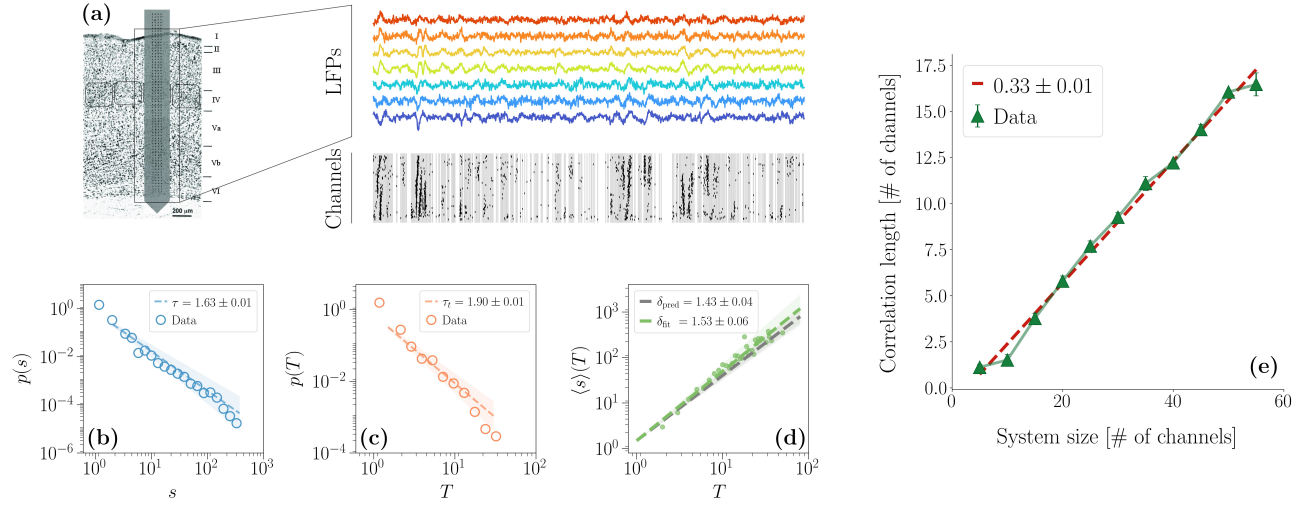


FIG. 1. (a) Left: scheme of the array used to obtain the LFPs data from all the cortical layers of the barrel cortex (modified from [40]); right an example of the LFPs signals for different layers and the corresponding discretization. An array of 256 channels organized in a  $64 \times 4$  matrix is inserted in a barrel column and the signals from the cortical layers are collected by  $55 \times 4$  electrodes. (b-d) Avalanche statistics obtained from the analysis of LFPs data in a rat. Both the distribution of the avalanches (b) sizes and (c) duration are power-laws, and (d) the crackling-noise relation is satisfied. (e) Scaling of the correlation length with the system size in LFPs data, averaging over four different rats. The error bars are shown as 5 standard deviations from the mean for visual ease. The correlation length scales linearly with the system size with no plateau in sight, a hallmark of criticality.

the scaling of the correlation length  $\xi$  as a function of the system sizes  $L$  [41, 46], we find that  $\xi$  scales linearly with  $L$ , signaling the presence of long-range correlations. This behavior matches exactly what would happen at a critical point, where the correlation length diverges in the thermodynamic limit and thus grows with the size of a finite system.

Hence, we find that the measured neural activity in the barrel cortex at rest displays two different signatures of criticality - power-law avalanches and scale-free spatial correlations. In order to try and unfold the underlying processes from which these collective properties emerge, we assume that neural activity may be decomposed in two parts [47, 48]: (i) the *intrinsic activity*, which is the activity driven by interactions between neurons or populations of neurons - in our case, the propagation dynamics across the multi-layer network of the interconnected neurons along the barrel; (ii) the *extrinsic activity*, which instead corresponds to the activity modulated by an external or global unit - in our case, the external inputs triggering or modulating the propagation (e.g. synaptic current injection from the thalamic inputs).

We introduce a paradigmatic model of  $N$  variables  $(v_1, \dots, v_N)$ , denoting the activity of  $N$  units (e.g. neurons or, as in our case, distinct populations of neurons as measured by our LFPs). This model is simple enough to be treated analytically and to provide a clear physical interpretation, while being complex enough to display non-trivial behaviors [49]. Focusing first on the extrinsic activity only, we model these variables as conditionally independent through an Ornstein-Uhlenbeck

(OU) process [50–53] with time-dependent diffusion

$$\frac{dv_i(t)}{dt} = -\frac{1}{\gamma_i} v_i(t) + \sqrt{\mathcal{D}(t)} \eta_i(t), \quad (1)$$

where  $\gamma_i$  is the characteristic time of the  $i$ -th neuron,  $\eta_i(t)$  is a white noise, and  $\mathcal{D}(t)$  corresponds to a noise strength modulation from an external input that is shared among all the units. In particular, we define the noise modulation  $\mathcal{D}(t)$  as

$$\mathcal{D}(t) = \begin{cases} \mathcal{D}^* & \text{if } D(t) \leq \mathcal{D}^* \\ D(t) & \text{if } D(t) > \mathcal{D}^* \end{cases} \quad (2)$$

where, following [19],  $D(t)$  is itself an OU process  $\dot{D}(t) = -D(t)/\gamma_D + \sqrt{\theta} \eta_D(t)$  [54]. Therefore, the noise modulation  $\mathcal{D}$  can be either constant in time and equal to  $\mathcal{D}^*$  or change in time according to an OU process with value  $D(t) > \mathcal{D}^*$ .

We now assume that the timescales of the two processes are separated [47], that is  $\gamma_D \gg \gamma_i$ , so that the stationary probability distribution of the activity is  $p(v) = \int d\mathcal{D} \prod_{i=1}^N p(v_i|\mathcal{D})p(\mathcal{D})$  and in general  $p(v_i, v_j) \neq p(v_i)p(v_j)$ . Thus, the presence of the unobserved modulation results in the emergence of an effective dependence between the units. Remarkably, one can show that the units, although not independent, are always uncorrelated  $\langle v_i v_j \rangle - \langle v_i \rangle \langle v_j \rangle = 0 \quad \forall i \neq j$  [41]. At the same time, the dependence between the units is shaped by the parameter  $\mathcal{D}^*$ . If  $\mathcal{D}^*$  is high enough, the modulation is rare and the units are always dominated by noise as we can see

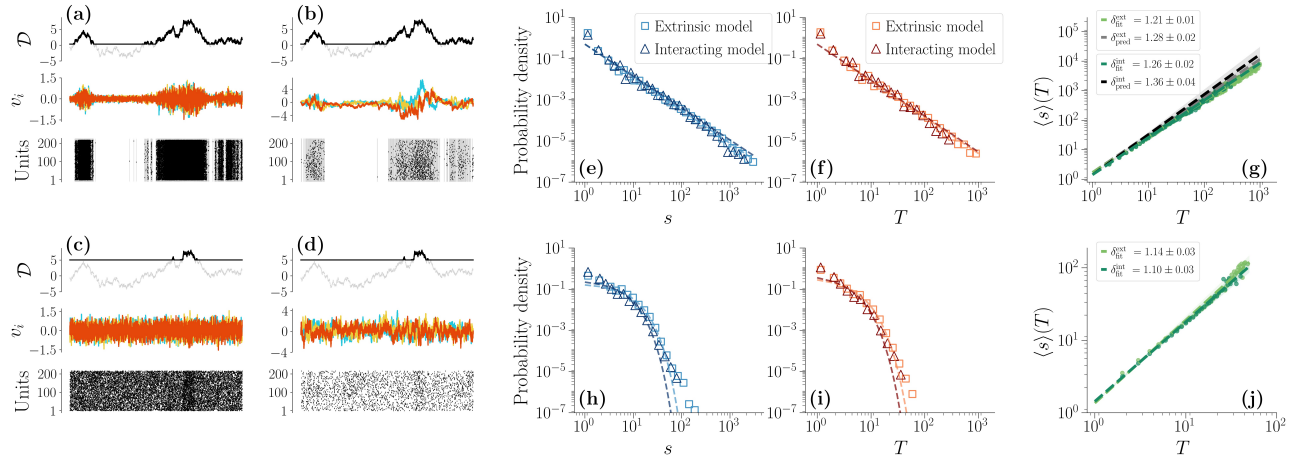


FIG. 2. Avalanche statistics generated by the model at  $\mathcal{D}^* = 0.3$  (a-b, e-g) and at  $\mathcal{D}^* = 5$  (c-d,h-j), with  $\gamma_D = 15$  and  $\theta = 1$  and  $\gamma_i = \gamma = 0.05$  for the extrinsic model. (a-b) Comparison between the trajectories of  $\mathcal{D}(t)$ ,  $v_i$  and the corresponding discretization in the low- $\mathcal{D}^*$  regime for (a) the extrinsic model and (b) the interacting one. (c-d) Same, but in the high- $\mathcal{D}^*$  regime. (e-g) If  $\mathcal{D}^*$  is low, avalanches are power-law distributed with almost identical exponents in the extrinsic and interacting model,  $\tau^{\text{ext}} = 1.60 \pm 0.01$ ,  $\tau^{\text{int}} = 1.55 \pm 0.01$  and  $\tau_t^{\text{ext}} = 1.77 \pm 0.01$ ,  $\tau_t^{\text{int}} = 1.74 \pm 0.01$ . The crackling-noise relation is verified in both cases. (h-j) Same plots, now in the high- $\mathcal{D}^*$  regime. Avalanches are now fitted with an exponential distribution. Notice that larger events, corresponding to periods in which  $\mathcal{D}(t) > \mathcal{D}^*$ , show up in the distributions' tails, suggesting that the shift between exponentials and power-laws is smooth. (j) The average avalanche size as a function of the duration scales with an exponent that, as  $\mathcal{D}^*$  increases, becomes closer to the trivial one  $\delta_{\text{fit}}^{\text{ext}} \approx \delta_{\text{fit}}^{\text{int}} \approx 1$ .

in Figure 2c. On the other hand, if  $\mathcal{D}^*$  is small, whenever  $\mathcal{D}(t) = \mathcal{D}^*$  the noise contribution to the units will be vanishing and the activity will follow an exponential decay. Therefore, in this regime, each  $v_i$  will typically alternate periods of quasi-silence to periods of activity. In other words, depending on the value of  $\mathcal{D}^*$ , this model can either reproduce a noise-driven behavior or a bursty, coordinated one, as shown in Figure 2a.

Most importantly, the low  $\mathcal{D}^*$  regime is also the onset of power-law distributed avalanches, as we see by simulating the model at different  $\mathcal{D}^*$  and performing the same analysis as in the LFP. We find that, as  $\mathcal{D}^*$  decreases, a transition between exponential decaying avalanches and power-law distributed ones appears. Figures 2e-f-g show that for  $\mathcal{D}^*$  small enough, the stochastic modulation produces scale-free avalanches in both size and time with exponents  $\tau^{\text{ext}} = 1.60 \pm 0.01$  and  $\tau_t^{\text{ext}} = 1.77 \pm 0.01$  satisfying the crackling-noise relation, i.e.  $\delta_{\text{fit}}^{\text{ext}} = 1.21 \pm 0.01 \approx \delta_{\text{pred}}^{\text{ext}} = 1.28 \pm 0.02$ . Moreover, the rescaled temporal profiles of these avalanches collapse to a single curve, as we show in the Supplemental Material [41]. On the other hand, for higher  $\mathcal{D}^*$  only exponential-decaying avalanches are present as we see in Figures 2h-i-j.

Although this is an archetypal example, our results are qualitatively unchanged if we use a more biological plausible model, at the price of losing analytical tractability. In particular, as shown in the Supplemental Material [41], we model the firing rates of both the external modulation and of the neural dynamics through non-interacting Wilson-Cowan units [55]. We set the external dynamics in a balanced state [56] and we still find that the avalanches of this extrinsic Wilson-Cowan model do dis-

play power law avalanches and the crackling noise relation is satisfied as well.

We have thus shown that avalanches statistics can be generated by non-critical mechanisms such as the one presented above. However the correlations as observed in Figure 1c cannot be explained by the extrinsic model. We thus introduce an intrinsic component in the OU model, i.e., we add a reconstructed effective connectivity [53] to Eqs. (S3-2). Namely, we now consider

$$\frac{dv_i(t)}{dt} = - \sum_j A_{ij} v_j(t) + \sqrt{\mathcal{D}(t)} \eta_i(t) \quad (3)$$

where  $A_{ij}$  is the effective connectivity matrix describing the interaction between the  $i$ -th and the  $j$ -th unit. Since in the extrinsic model the units are uncorrelated, we show in the Supplemental Material [41] that we can infer the values of  $A_{ij}$  directly from the data, by solving the inverse problem in such a way that the correlations of Eq. (3) match the experimentally-measured correlations  $\sigma_{ij}$  of our LFPs. The different regimes for the interacting model are plotted in Figures 2b and 2d.

As shown in Figures 2e-f-g, all avalanches exponents  $\tau \approx 1.6$ ,  $\tau_t \approx 1.75$  and  $\delta \approx 1.28$  are not changed significantly by the inclusion of direct interactions among the units, nor the high  $\mathcal{D}^*$  regime is changed either as shown in Figures 2h-i-j. Let us note that these exponents are different from the ones obtained in LFP data, but this is perhaps not surprising. In fact, beside the simplicity of this paradigmatic model, such exponents have been found to depend on the experimental settings [30] and on individual variability [22]. Nevertheless, our

framework reproduces the ubiquitous scaling exponent  $\delta \approx 1.28$  [22, 39], which we also find in our experimental settings in MUAs data [43].

The fact that the exponents do not change when we add the interaction network to our model has a profound implication: if we measure neural avalanches alone, we might not be able to infer anything on the intrinsic neural dynamics of our model. However, we might have access to such dynamics if we investigate the correlations of the fluctuations. This disentangling is deeply related to the dependency structure of our model, described by the mutual information

$$I = \int_{-\infty}^{+\infty} dv_i \int_{-\infty}^{+\infty} dv_j p(v_i, v_j) \log \frac{p(v_i, v_j)}{p(v_i)p(v_j)}, \quad (4)$$

which captures pairwise dependencies in the system that go well beyond simple correlations. In Figure 3a we show that a non-zero mutual information emerges in the extrinsic model in the low  $\mathcal{D}^*$  limit. The onset of the coordinated behavior between the units, i.e., of power-law distributed avalanches, is also the onset of a non-zero mutual information. When interactions are added back, the mutual information is simply shifted independently of  $\mathcal{D}^*$  [41], signaling that the effects of external modulation and the effective interactions are completely disentangled [57].

Furthermore, with the effective interactions reconstructed from the data we can also study the scaling of the correlation length  $\xi$  as a function of the system sizes  $L$  and we plot the result in Figure 3b. As in our data,  $\xi$  scales linearly with  $L$  in the interacting model, displaying thus a signature of criticality that not only is strictly dependent on the interaction network, but that is also completely unaffected by avalanches. In fact, as with the mutual information, the correlations in the interacting model scale trivially with  $\mathcal{D}^*$  and thus the correlation length is not affected by  $\mathcal{D}^*$  (see the Supplemental Material [41]).

Overall, our work shows that while power-law avalanches and the crackling-noise relation both appear in LFPs data from the rat's barrel cortex, their relation with criticality is far from stringent. We have developed a paradigmatic, but of analytical ease, framework where the intrinsic contributions to the neuronal activity, due to the direct interaction between the units themselves, and the extrinsic ones, arising from externally-driven modulated activity, are exactly disentangled. Our model displays a regime in which power-law avalanches that satisfy the crackling-noise relation emerge and that are compatible with the universal exponent  $\delta \approx 1.28$  that appears in [22], a general result that holds also when considering a different extrinsic model, such as Wilson-Cowan units. The fact that this exponent turns out to be so ubiquitous in a variety of neural systems, from freely moving or anesthetized mammals to cultured slices, suggests that it could be explained by some basic phenomena shared by all these systems. We propose that such phenomena can be represented by a simple time varying extrinsic dy-

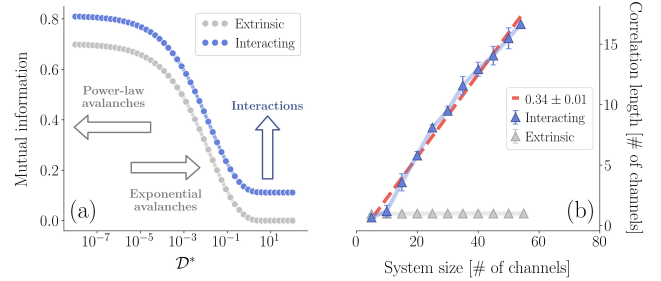


FIG. 3. (a) Comparison between the mutual information in the extrinsic model ( $\theta = 1$ ,  $\gamma_D = 10$ ,  $\gamma_1 = 0.1$ ,  $\gamma_2 = 0.5$ ) and, as an example, in the interacting model with two units (see the Supplemental Material [41]). Notice that the onset of a non-vanishing mutual information induced by  $\mathcal{D}(t)$  is also the onset of power-law distributed avalanches, whereas the mutual information arising from interactions is independent on  $\mathcal{D}^*$ . (b) The correlation length of the interacting model scales linearly with the system size, as in the data. In the extrinsic model, as expected, the correlation length of the fluctuations is constant and equal to 1, i.e., the correlation function drops to zero for adjacent electrodes.

namics that does not require any fine tuning to criticality [24].

At the same time, we show that in spatially-extended LFPs data seemingly scale-free spatial correlations are present. While they can coexist with phenomena like power-law avalanches, these kind of signatures are not explained by the extrinsic activity alone and thus may be deeply related to the origin of criticality in the brain, playing a fundamental role in the advantages it might achieve by being critical [3, 9, 58, 59]. Crucially, our archetypal model allows to combine this extrinsic dynamics to an intrinsic interaction matrix, inferred directly from the experimental data to match the seemingly scale-free spatial correlations we find in our experiments. When we do so, we show that these two signatures of criticality are completely disentangled - avalanches appear as a sole consequence of the external modulation and are not affected by the interactions, and, vice-versa, the interactions determine the spatial correlations independently on the external modulation.

Remarkably, it was recently shown that in these kind of models the mutual information always receives distinct and disentangled contributions from the internal interactions and from an environmental, external dynamics [57]. Although, clearly, the presence of a non-zero mutual information cannot be a sufficient condition for power-law avalanches to appear, in our extrinsic model their emergence does correspond to the onset of a non-vanishing mutual information. This fact suggests a promising future perspective. By explicitly considering both the intrinsic activity and the extrinsic contributions, one might be able to combine all these considerations into a unified information-theoretic view - and perhaps helping to unfold the underlying biological mechanisms at the origin of the observed signatures of criticality in neural activity.





- don, Academic press, third ed., 2003.
- [62] C. W. Gardiner, *Handbook of stochastic methods for physics, chemistry and the natural sciences*, vol. 13 of *Springer Series in Synergetics*. Springer-Verlag, third ed., 2004.
- [63] Let us note that the process is simulated through its discrete version by employing the Euler–Maruyama method [60], and for this purpose a finite  $dt$  has to be chosen. The deterministic part of the discrete version of the process is a discrete map of the form  $\mathbf{v}(t + dt) = K\mathbf{v}(t)$ , where  $K = \mathbb{I} + (W - \frac{\mathbb{I}}{\gamma})dt$ . When choosing  $dt$  one has to ensure that  $K$  has spectral radius less than unity, in order to guarantee stability.
- [64] R. H. Bartels and G. W. Stewart, “Solution of the matrix equation  $AX + XB = C$ ,” *Commun. ACM*, vol. 15, no. 9, p. 820–826, 1972.
- [65] D. A. Martin, T. L. Ribeiro, S. A. Cannas, T. S. Grigera, D. Plenz, and D. R. Chialvo, “Box scaling as a proxy of finite size correlations,” *Scientific Reports*, vol. 11, no. 1, pp. 1–9, 2021.
- [66] W. Shew, W. Clawson, J. Pobst, and al, “Adaptation to sensory input tunes visual cortex to criticality.,” *Nature Phys.*, vol. 11, p. 659–663, 2015.
- [67] G. Buzsáki, C. Anastassiou, and C. Koch, “The origin of extracellular fields and currents — EEG, ECoG, LFP and spikes,” *Nature Review Neuroscience*, vol. 13, pp. 407–420, 2012.
- [68] A. Clauset, C. R. Shalizi, and M. E. J. Newman, “Power-law distributions in empirical data,” *SIAM Rev.*, p. 661–703, 2009.
- [69] K. Bansal, J. O. Garcia, N. Lauharatanahirun, S. F. Muldoon, P. Sajda, and J. M. Vettel, “Scale-specific dynamics of large-amplitude bursts in eeg capture behaviorally meaningful variability,” 2020.
- [70] N. Marshall, N. M. Timme, N. Bennett, M. Ripp, E. Lautzenhiser, and J. M. Beggs, “Analysis of power laws, shape collapses, and neural complexity: New techniques and matlab support via the ncc toolbox,” *Frontiers in Physiology*, vol. 7, p. 250, 2016.
- [71] S. Scarpetta, I. Apicella, L. Minati, and A. de Canidia, “Hysteresis, neural avalanches, and critical behavior near a first-order transition of a spiking neural network,” *Phys. Rev. E*, vol. 97, p. 062305, 2018.
- [72] L. M. Ricciardi and L. Sacerdote, “The ornstein-uhlenbeck process as a model for neuronal activity,” *Biological cybernetics*, vol. 35, no. 1, pp. 1–9, 1979.
- [73] N. Brunel, “Dynamics of sparsely connected networks of excitatory and inhibitory spiking neurons,” *Journal of Computational Neuroscience*, vol. 8, p. 183–208, 2000.

# Supplemental Material for “On the critical signatures of neural activity”

## A. EXPERIMENTAL SETTING

### 1. Surgical procedures

LFPs recordings are performed on Wistar rats, which are maintained under standard environmental conditions in the animal research facility of the Department of Biomedical Sciences of the University of Padova. All the procedures are approved by the local Animal Care Committee (O.P.B.A.) and the Italian Ministry of Health (authorization number 522/2018-PR). Young adult rats aged 36 to 43 days and weighting between 150 and 200 g are anesthetized with an intra-peritoneal induction mixture of tiletamine-xylazine (2 mg and 1.4 g/100 g body weight, respectively), followed by additional doses (0.5 mg and 0.5 g/100 g body weight) every hour. The anesthesia level is constantly monitored by testing the absence of eye and hind-limb reflexes and whiskers' spontaneous movements. Each animal is positioned on a stereotaxic apparatus where the head is fixed by teeth- and ear-bars. To expose the cortical area of interest, an anterior-posterior opening in the skin is made in the center of the head and a window in the skull is drilled over the somatosensory barrel cortex at stereotaxic coordinates  $-1 \div -4$  AP,  $+4 \div +8$  ML referred to bregma [61]. A slit in the meninges is then carefully made with fine forceps at coordinates  $-2.5$  AP,  $+6$  ML for the subsequent insertion of the recording probe. As a reference, the depth is set at  $0 \mu\text{m}$  when the electrode proximal to the chip tip touches the cortical surface. The neuronal activity is recorded from the entire barrel cortex (from  $0$  to  $-1750 \mu\text{m}$ ), which is constantly bathed in Krebs' solution (in mM: NaCl 120, KCl 1.99, NaHCO<sub>3</sub> 25.56, KH<sub>2</sub>PO<sub>4</sub> 136.09, CaCl<sub>2</sub> 2, MgSO<sub>4</sub> 1.2, glucose 11). An Ag/AgCl electrode bathed in the extracellular solution in proximity of the probe is used as reference.

### 2. Recordings

LFPs are recorded through a custom-made needle which integrates a high density array, whose electrodes are organized in a  $64 \times 4$  matrix. The operation principle of the multi-electrode-arrays used to record LFPs is an extended CMOS based EOSFET (Electrolyte Oxide Semiconductor Field Effect Transistor). The recording electrodes are  $7.4 \mu\text{m}$  in diameter size and the needle is  $300 \mu\text{m}$  in width and  $10\text{mm}$  long. The x- and y-pitch (i.e. the distance between adjacent recording sites) are  $32 \mu\text{m}$ . The multiplexed signals are then digitized by a NI PXIe-6358 (National Instruments) up to  $1.25\text{MS/s}$  at 16bit resolution and saved to disk by a custom LabVIEW acquisition software. The LFP signal is sampled at  $976.56$  Hz and band-pass filtered (2-300 Hz). The dataset analyzed for this work consist in 20 trials of basal activity lasting 7.22 seconds, that are recorded from 4 rats.

### 3. Barrel cortex

The barrel cortex is the region of the primary somatosensory cortex (S1) that encodes tactile sensory inputs from the rodents' whiskers. The barrel presents a high degree of segmentation into vertical columns and horizontal layers. The whisker-related barrel column is a cylindrical structure spanning vertically the six layers of the barrel cortex, although its border is defined exclusively by spatially aligned sub-cellular structures in layer 4 called barrels.

Each barrel-column is composed of an archetypal circuit that is repeated in each column. Importantly, the barrels are laid out in a pattern that is nearly identical to the whiskers on the rat's snout that, together with the underlying neural circuit, suggests a highly specific correspondence between whiskers and barrel columns.

## B. THE EXTRINSIC MODEL

As explained in the main text, we introduce a model of  $N$  variables ( $v_1, \dots, v_N$ ) that are conditionally independent given the state of the external input. In particular, let us assume that there are some parameters  $\xi = (\xi_1, \dots, \xi_M)$  controlling the extrinsic modulation, that is

$$p(v_i, v_j, t | \xi) = p(v_i, t | \xi) p(v_j, t | \xi) \quad \forall i, j. \quad (\text{S1})$$

Since at this moment we assume no direct interaction is happening, we think about the probability distribution  $p(v_i | \xi)$  as shaped by extrinsic activity alone. That is, once we specify  $\xi$ , no interaction happens between the  $i$ -th variable

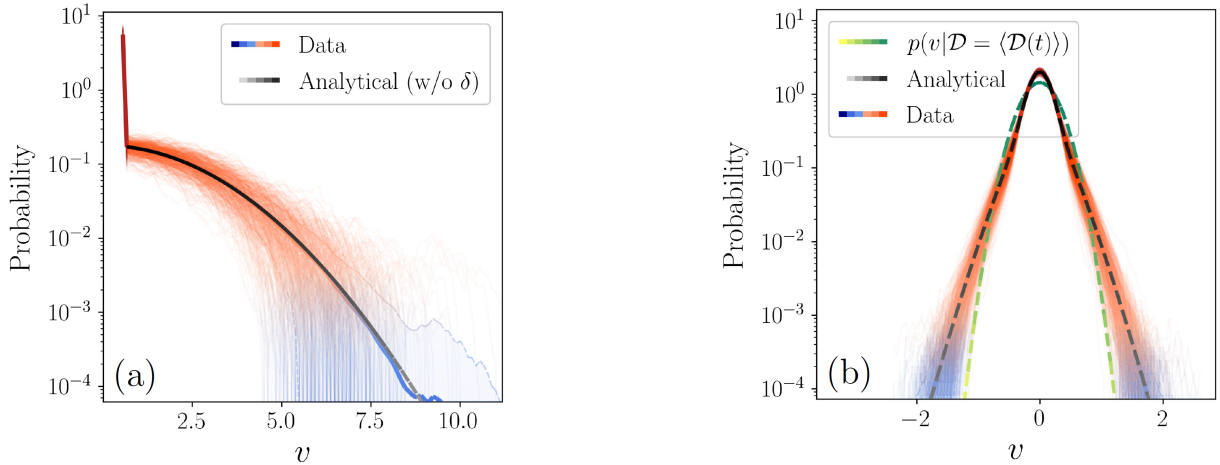


FIG. S1. Comparison between the stationary distributions obtained in the main text and the results  $10^3$  simulations. Semi-transparent lines represent different simulations. Filled areas of the plots represent one standard deviation from the mean distribution. (a) Probability distribution of  $\mathcal{D}$ . (b) Probability distribution of a single  $v_i$ .

and the  $j$ -th variable. However, we now suppose that we do not have access on the states of the external parameters. Hence, we can only hope of describing to the joint probability distribution

$$p(v_1, \dots, v_N, t) = \int d\xi \prod_{i=1}^N p(v_i, t | \xi) p(\xi, t) \quad (\text{S2})$$

which is what we typically observe in an experimental setting. In general, due to the marginalization over the external parameters this probability distribution is not factorizable, and thus in this sense it is not trivial.

In general, we want to work in the stationary limit and thus there is a complication we need to take into account. In particular, since the integrand of Equation (S2) can be arbitrarily complicated, we would like to be able to perform the stationary limit before the marginalization, i.e,

$$\lim_{t \rightarrow \infty} p(v_1, \dots, v_N, t) = \int d\xi \prod_{i=1}^N \lim_{t \rightarrow \infty} p(v_i, t | \xi) \cdot \lim_{t \rightarrow \infty} p(\xi, t).$$

This limit, of course, is not always true, but it does hold if we assume that the time-scales of the two processes - the process for  $\mathbf{v}$  and for  $\xi$  - are separated. In particular, we are interested in the limit in which the timescale of  $\xi$  is slower than  $\mathbf{v}$ , so that  $\mathbf{v}$  relaxes to its stationary state in a time-frame in which the external modulation can be considered constant.

Let us now describe the particular choices of the main text, where

$$\frac{dv_i(t)}{dt} = -\frac{1}{\gamma_i} v_i(t) + \sqrt{\mathcal{D}(t)} \eta(t) \quad (\text{S3})$$

is the process that generates  $\mathbf{v}$  and the single-parameter external modulation is

$$\mathcal{D}(t) = \begin{cases} \mathcal{D}^* & \text{if } \mathcal{D}(t) \leq \mathcal{D}^* \\ D(t) & \text{if } \mathcal{D}(t) > \mathcal{D}^* \end{cases} \quad (\text{S4})$$

where

$$\frac{dD(t)}{dt} = -\frac{1}{\gamma_D} D(t) + \sqrt{\theta} \eta(t). \quad (\text{S5})$$

For the above considerations to hold, we assume that  $\gamma_D \gg \gamma_i$ . This is simply a time-scale separation limit. In this limit, the process of  $v_i$  reaches stationarity much faster than the process of  $\mathcal{D}$ , thus the overall stationary distribution is the stationary distribution  $p(v_i | \mathcal{D})$  averaged over the stationary distribution  $p(\mathcal{D})$ . Hence we have

$$p(\mathcal{D}) = \frac{1}{2} \left[ 1 + \text{Erf} \left( \frac{\mathcal{D}^*}{\sqrt{\theta \gamma_D}} \right) \right] \delta(\mathcal{D} - \mathcal{D}^*) + \frac{H(\mathcal{D} - \mathcal{D}^*)}{\sqrt{\pi \theta \gamma_D}} e^{-\frac{\mathcal{D}^2}{\theta \gamma_D}}, \quad (\text{S6})$$

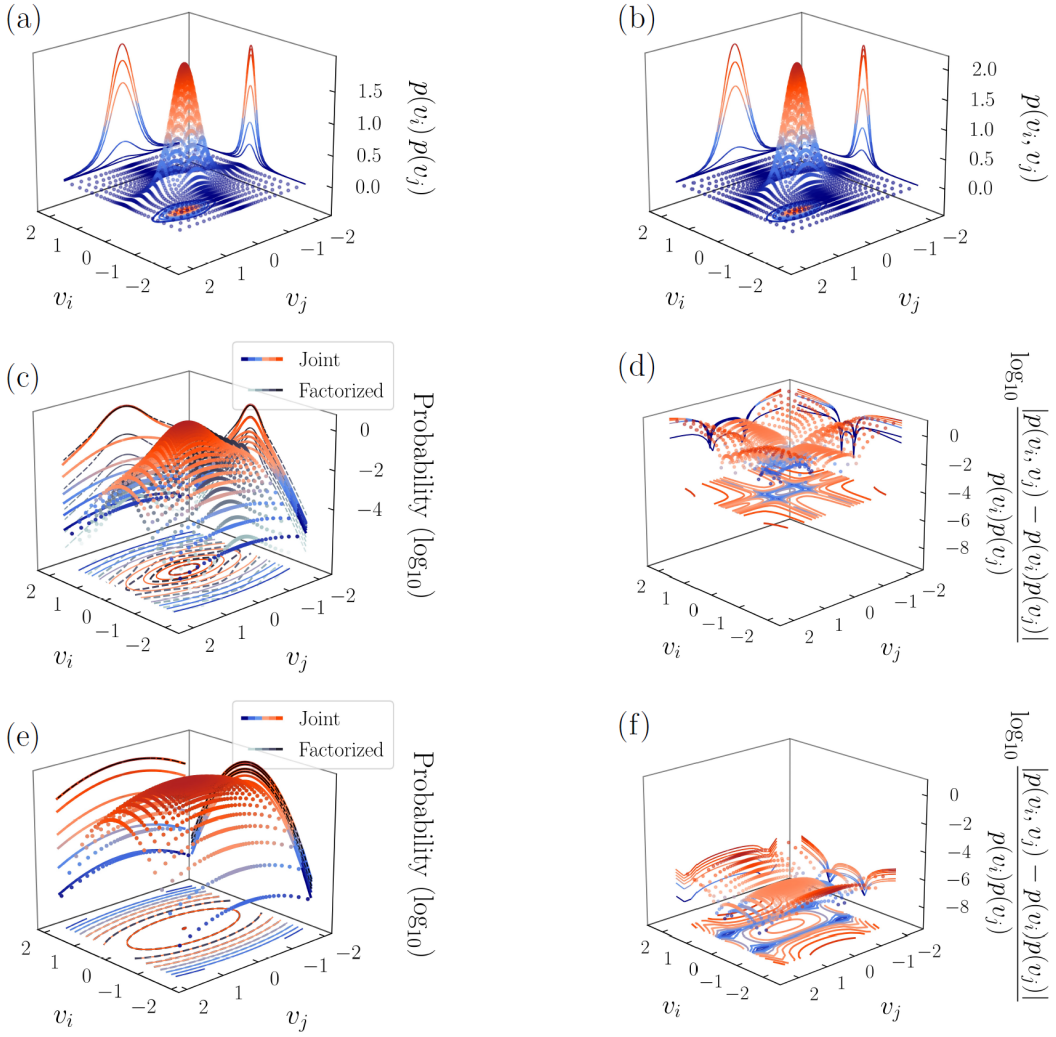


FIG. S2. Comparison between the analytical expressions of the joint probability distribution in Eq. (S8) and its factorization  $p(v_i, v_j)$ . (a) The factorized distribution. (b) The joint distribution. (c) Comparison between the two in a log-plot. (d) Relative difference between the two with respect to the factorized distribution. (e-f) Comparison between the joint and the factorized distributions, with the same parameters except for  $D^* = 5$ .

where  $H$  is the Heaviside step function. Then, the computation of the stationary probability distributions is quite easy. The single-unit probability is given by

$$\begin{aligned} p(v_i) &= \int d\mathcal{D} p(v_i|\mathcal{D}) p(\mathcal{D}) = \int d\mathcal{D} \frac{1}{\sqrt{\pi\gamma_i\mathcal{D}}} e^{-\frac{v_i^2}{\gamma_i\mathcal{D}}} p(\mathcal{D}) \\ &= \frac{1 + \text{Erf}\left(\frac{\mathcal{D}^*}{\sqrt{\theta\gamma_D}}\right)}{2\sqrt{\pi\mathcal{D}^*\gamma_i}} e^{-\frac{v_i^2}{\mathcal{D}^*\gamma_i}} + \frac{1}{\sqrt{\pi^2\theta\gamma_D\gamma_i}} \int_{\mathcal{D}^*}^{\infty} d\mathcal{D} \frac{1}{\sqrt{\mathcal{D}}} e^{-\left[\frac{\mathcal{D}^2}{\theta\gamma_D} + \frac{v_i^2}{\mathcal{D}\gamma_i}\right]} \end{aligned} \quad (\text{S7})$$

and, in principle, we can compute the probability distributions for any number of variables  $\{v_i\}$  in the same way.

We note that although before the marginalization the two-point probability distribution is factorizable

$$p(v_i, v_j, \mathcal{D}) = p(v_i, v_j|\mathcal{D}) p(\mathcal{D}) = p(v_i|\mathcal{D}) p(v_j|\mathcal{D}) p(\mathcal{D}),$$

the marginalization itself breaks the factorization, namely

$$\int d\mathcal{D} p(v_i, v_j, \mathcal{D}) \neq \left[ \int d\mathcal{D} p(v_i, \mathcal{D}) \right] \left[ \int d\mathcal{D} p(v_j, \mathcal{D}) \right].$$

Hence, we can write down the two-unit joint probability as

$$p(v_i, v_j) = \frac{1 + \text{Erf}\left(\frac{\mathcal{D}^*}{\sqrt{\theta\gamma_D}}\right)}{2\pi\mathcal{D}^*\sqrt{\gamma_i\gamma_j}} e^{-\frac{1}{\mathcal{D}^*}\left(\frac{v_i^2}{\gamma_i} + \frac{v_j^2}{\gamma_j}\right)} + \frac{1}{\sqrt{\gamma_i\gamma_j\gamma_D\pi^3\theta}} \int_{\mathcal{D}^*}^{\infty} \frac{dD}{D} e^{-\frac{1}{D}\left(\frac{v_i^2}{\gamma_i} + \frac{v_j^2}{\gamma_j}\right)} e^{-\frac{D^2}{\theta\gamma_D}} \quad (\text{S8})$$

where the second term is not factorizable.

From these probabilities we can immediately show that

$$\langle v_i v_j \rangle - \langle v_i \rangle \langle v_j \rangle = 0 \quad \forall i \neq j \quad (\text{S9})$$

and, in general, all the expectation values where a variable  $v_i$  appears an odd number of times vanish. This follows from the simple fact that, for instance,

$$\langle v_i v_j \rangle = \int dv_i dv_j p(v_i, v_j) v_i v_j = \int d\mathcal{D} p(\mathcal{D}) \left( \int dv_i v_i p(v_i | \mathcal{D}) \right) \left( \int dv_j v_j p(v_j | \mathcal{D}) \right) = 0 \quad \forall i \neq j$$

since  $\int dv_i v_i p(v_i | \mathcal{D}) = 0$ . In fact, let us note that this is not a general feature of these kind of models, but it is rather a property inherited from the choice of an OU process for  $v_i$  given  $\mathcal{D}$ , for which all the odds moment vanish. The diagonal entries of the covariance matrix, on the other hand, are given by

$$\langle v_i^2 \rangle = \frac{\gamma_i \mathcal{D}^*}{2} \left[ 1 + \text{Erf}\left(\frac{\mathcal{D}^*}{\sqrt{\theta\gamma_D}}\right) \right] + \sqrt{\frac{\gamma_i^2 \theta \gamma_D}{16\pi}} e^{-\frac{(\mathcal{D}^*)^2}{\theta\gamma_D}}$$

Thus, in this particular setting, the units are uncorrelated and have a variance that is independent on the other units. At the same time, however, it is clear that in general  $p(v_i, v_j) \neq p(v_i)p(v_j)$  so while uncorrelated the variables are not independent.

### C. TESTING THE PREDICTIONS OF THE EXTRINSIC MODEL

We now show that simulations of the extrinsic model described by Equation S3 agree with the analytical results. Whenever not specified, we assume that the parameters of the model are given by  $\mathcal{D}^* = 0.3$ ,  $\theta = 1$ ,  $\gamma_D = 10$  together with  $\gamma_i = 0.1$ ,  $\gamma_j = 0.5$ . Thus, we are in the limit of timescale separation considered in the main text.

Let us begin with Figure S1. Albeit trivial, we first check in Figure S1a that the stationary distribution of  $\mathcal{D}$  is indeed the one of Eq. (S6) and in Figure S1b that the stationary distribution of a single  $v_i$  does correspond to the analytical expression of Eq. (S7). If we compare this distribution to a standard distribution of an Ornstein-Uhlenbeck process with a diffusion coefficient equal to the mean  $\langle \mathcal{D}(t) \rangle$  [54] we immediately see that the distribution of our model is considerably more peaked around zero and displays longer tails. Indeed, one expects that due to the fact that  $\mathcal{D}^* < \langle \mathcal{D}(t) \rangle$  the system tends to wander more easily close to zero, especially in the time windows where the diffusion coefficient is constant and equal to  $\mathcal{D}^*$ . At the same time, the fact that  $\mathcal{D}(t)$  can change in time favors the presence of values of  $v$  that are larger in absolute value, which is the mechanism at the origin of the bursty behavior seen in the main text.

In Figure S2 we look instead at the properties of the joint probability distribution  $p(v_i, v_j)$ . The most natural quantity to compare this distribution with is its factorization  $p(v_i)p(v_j)$ , which is equivalent to ignoring the feedback effects between  $v_i$  and  $v_j$  due to the shared extrinsic modulation of  $\mathcal{D}(t)$ . Since we are setting  $\mathcal{D}^* = 0.5$ , we expect that these effects are going to be particularly relevant for the dynamics of the model. In particular, in Figure S2c-d we see that the most important differences between the two occur in the tails of the two-dimensional distribution, with the joint distribution typically showing dramatically longer tails. This translates to the fact that far-from-zero values of the two variables can occur more easily at the same time.

The situation is completely reversed when we increase  $\mathcal{D}^*$ . In Figure S2e-f we see that for  $\mathcal{D}^* = 8$  the joint probability distribution and the factorized distribution are almost indistinguishable. Hence, this example shows explicitly that if  $\mathcal{D}^*$  is high enough the dependence induced by the extrinsic modulation vanishes.

Let us keep focusing on the case  $\mathcal{D}^* = 0.5$  for the time being. In Figure S3a-d we compare the one-dimensional sections of the analytical expression of the joint probability distribution with the results of  $10^3$  simulations of the model, together with the sections of the factorized distribution. The joint distribution estimated from the simulation matches particularly well the analytical prediction. Once more, and perhaps more clearly, in Figure S3a-b we see the stark difference that emerges along the tails between the joint probability distribution and its factorization. Interestingly, panel (c) and panel (d) show that the situation in the bulk of the distribution is reversed with respect to

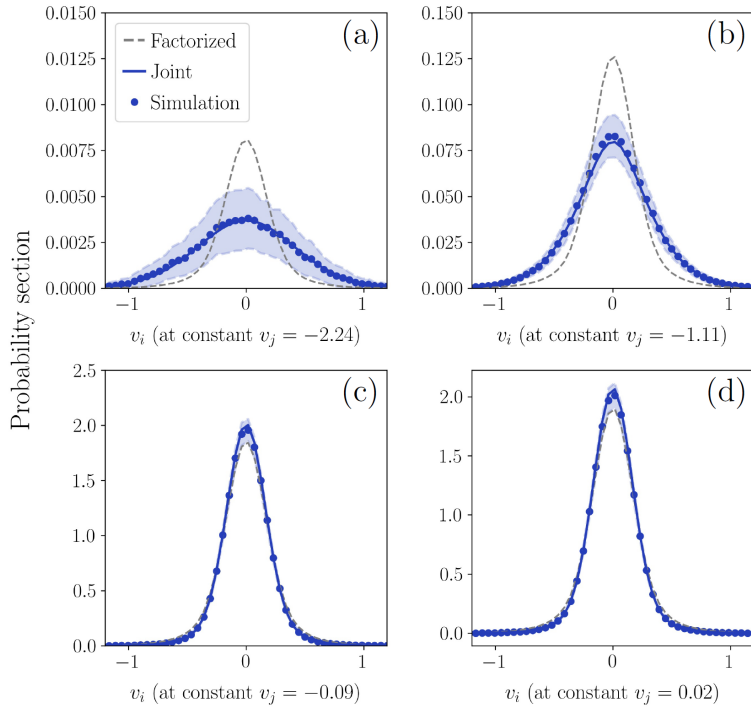


FIG. S3. Comparison between the analytical expressions of the joint probability distribution  $p(v_i, v_j)$  given by Eq. (S8) and the one obtained from  $10^3$  simulations. We also show the corresponding results for the factorized probabilities. The blue line corresponds to the analytical expression of  $p(v_i, v_j)$ . The corresponding dots represent the histogram of the distribution obtained from  $10^3$  simulations, and the semitransparent filled areas represent one standard deviation from this estimate. Similarly, the gray dashed line represent the analytical expression of  $p(v_i)p(v_j)$ . (a) Section along the  $v_j$  direction for small  $v_j$ , so that we are looking at the tails of the distribution. Even though the estimate along the tails is noisy, we clearly see that the estimate from the simulations lies along the analytical prediction. (b) As before, but for higher  $v_j$ . (c-d) As before, but with values of  $v_j$  close to zero so we look at the bulk of the distribution near its peak. Even though joint probability and its factorization now are more similar, once more the estimate from the simulation match the analytical expression  $p(v_i, v_j)$ .

the tails and now the joint probability distribution is more peaked with respect to its factorization, albeit only slightly. That is, the modulation in the low  $\mathcal{D}^*$  regime favors both large values of  $v_i$  and  $v_j$  and values very close to zero.

Overall, this brief analysis showed us how the bursty behavior that we see for small values of  $\mathcal{D}^*$  emerges from the underlying probability distributions, which in turn emerge from the simple marginalization that occurs in Eq. (S2). Similar arguments, albeit impractical, could be carried out for the probability distributions beyond the two-point ones. In a sense, one could argue that the fundamental properties of the model are inherited from the fact that there are some unobserved physical quantities, and these are the quantities that drive the global response of the single variables.

For the specific case of a double Ornstein-Uhlenbeck process we chose, the net effect of the marginalization is the widening of the tails of both the one-point  $p(v)$  and the two-point  $p(v_i, v_j)$  probability distributions when  $\mathcal{D}^*$  is small enough. As we increase  $\mathcal{D}^*$ , this effect becomes less and less important until it is completely negligible. In this sense, we can effectively think of  $\mathcal{D}^*$  as a control parameter that changes the qualitative behavior of the system. Most importantly, the fact that the tails of the joint probability distribution are wider when  $\mathcal{D}^*$  is small reflects dynamically in the emergence of a non trivial coordination between the variables, from which in turn power-law avalanches emerge.

#### D. THE MULTIVARIATE ORNSTEIN-UHLENBECK PROCESS

The process studied in the main text is a multivariate Ornstein-Uhlenbeck process [62] of the form

$$d\mathbf{v}(t) = -A\mathbf{v}(t)dt + B(t)d\mathbf{W}(t), \quad (\text{S10})$$

where in our case  $B(t)$  is a diagonal matrix whose diagonal elements are given by  $\sqrt{\mathcal{D}(t)}$ . In the case of decoupled units, which we use to model the extrinsic activity, the matrix  $A$  is again diagonal with entries  $A_{ij} = \delta_{ij}/\gamma_i$ . The

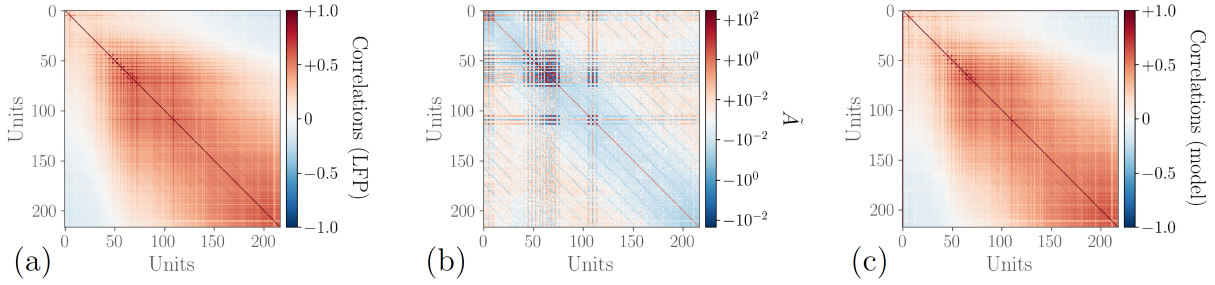


FIG. S4. Comparison between (a) the correlations of the data and (c) the correlations of the interacting model after solving the inverse problem. Panel (b) shows the inferred matrix  $\tilde{A}$ , which is independent on the parameters of the model.

formal solution of this stochastic process is given by

$$\mathbf{v}(t) = \exp(-At) \mathbf{v}(0) + \int_0^t \exp[-A(t-t')] B(t') d\mathbf{W}(t').$$

In particular, since in our case the matrix  $B$  is on itself a stochastic variable, from now on we will focus on the original variables conditioned on  $B$ , which in turn we assume follows its own stationary distribution  $p(B)$ . We call these conditioned variables  $\mathbf{v}(t, B)$ . If the eigenvalues of  $A$  have all positive real parts, a stationary solution of Eq. S10 exists and it is of the form [63]

$$\mathbf{v}_s(t, B) = \int_{-\infty}^t \exp[-A(t-t')] B d\mathbf{W}(t').$$

Hence, the stationary covariance matrix conditioned on  $B$  reads as

$$\begin{aligned} \sigma(B) &= \langle \mathbf{v}_s(t, B), \mathbf{v}_s^T(t, B) \rangle \\ &= \int_{-\infty}^t dt' \exp[-A(t-t')] B B^T \exp[A^T(t-t')] \end{aligned}$$

which solves the algebraic equation

$$A\sigma(B) + \sigma(B)A^T = M,$$

where the matrix  $M$  is given by

$$M = \int_{-\infty}^t A \exp[-A(t-t')] B B^T \exp[-A^T(t-t')] dt' + \int_{-\infty}^t \exp[-A(t-t')] B B^T \exp[-A^T(t-t')] A^T dt'.$$

We can rewrite it as

$$M = \int_{-\infty}^t \frac{d}{dt'} \{ \exp[-A(t-t')] B B^T \exp[-A(t-t')] \} dt'$$

Carrying out the integral, we find that the lower limit vanishes due to the assumed positivity of the eigenvalues of  $A$  and hence only the upper limit remains, giving

$$A\sigma(B) + \sigma(B)A^T = BB^T, \quad (\text{S11})$$

which is a continuous Lyapunov equation [64] for the covariance matrix  $\sigma(B)$  [53]. Then, we only need to marginalize over  $B$  and we obtain the equation for the covariance matrix of our original variables  $\mathbf{v}_s(t)$

$$A\sigma + \sigma A^T = Q, \quad (\text{S12})$$

where for the sake of brevity we call  $\sigma$  the covariance matrix of the original variables and  $Q$  is a diagonal matrix whose elements are given by

$$Q_{ij} = \delta_{ij} \int_{\mathcal{D}^*}^{\infty} \mathcal{D} p(\mathcal{D}) d\mathcal{D} := \delta_{ij} f(\mathcal{D}^*, \gamma_D, \theta). \quad (\text{S13})$$

Then, taking the transpose of Eq. (S12), and assuming that the matrix  $A$  is symmetric, we end up with a Lyapunov equation for the matrix  $A$ . Thus, the inverse problem of reconstructing the connectivity matrix from the data reduces to solving numerically  $\sigma A + A\sigma = Q$ , starting from the correlation matrix of the data and given a set of parameters for the model.

Hence we end up with a model

$$\dot{v}_i(t) = - \sum_j A_{ij} v_j(t) + \sqrt{\mathcal{D}(t)} \xi_i(t) \quad (\text{S14})$$

where  $A_{ij}$  depends on the the parameters of the stochastic modulation  $(\mathcal{D}^*, \gamma_D, \theta)$ . Notice that if we write  $\tilde{A}_{ij} = A_{ij}/f(\mathcal{D}^*, \gamma_D, \theta)$  we need to solve the Lyapunov equation  $\sigma \tilde{A} + \tilde{A}\sigma = \mathbb{W}$  that only depends on  $\sigma$ , the correlation matrix of the data. If we introduce  $\tilde{\mathcal{D}} = \mathcal{D}/f$  and  $\tilde{v}_i = v_i/\sqrt{f}$  we can write

$$\dot{\tilde{v}}_i(t) = - \sum_j \tilde{A}_{ij} \tilde{v}_j(t) + \sqrt{\tilde{\mathcal{D}}(t)} \xi_i(t)$$

and clearly

$$\langle \tilde{v}_i \tilde{v}_j \rangle - \langle \tilde{v}_i \rangle \langle \tilde{v}_j \rangle = \frac{\langle v_i v_j \rangle - \langle v_i \rangle \langle v_j \rangle}{f}$$

so the correlation between  $\tilde{v}_i$  and  $\tilde{v}_j$  is proportional to the correlation between  $v_i$  and  $v_j$ . This means that at different  $(\mathcal{D}^*, \theta, \gamma_D)$  we simply find a rescaled interaction matrix  $A_{ij}$ , but the scaling of correlation length does not change.

The stationary probability distribution solution of the interacting model can be written, in general, as

$$p(v_1, \dots, v_N) = \frac{1 + \text{Erf} \left[ \frac{\mathcal{D}^*}{\sqrt{\theta \gamma_D}} \right]}{2\sqrt{(\pi \mathcal{D}^*)^N \det \Sigma}} e^{-\frac{1}{\mathcal{D}^*} \mathbf{v}^T \Sigma^{-1} \mathbf{v}} + \frac{1}{\sqrt{(\gamma_D \theta)^N \pi^{N+1} \det \Sigma}} G_N \left( \frac{\mathcal{D}^*}{\sqrt{\theta \gamma_D}}, \frac{\mathbf{v}^T \Sigma^{-1} \mathbf{v}}{\sqrt{\theta \gamma_D}} \right) \quad (\text{S15})$$

where  $(A\Sigma + \Sigma A^T)/2 = \mathbb{W}$  and

$$G_N(\alpha, \beta) = \int_{\alpha}^{\infty} \frac{dx}{x^{N/2}} e^{-\frac{\beta}{x} - x^2}. \quad (\text{S16})$$

In general we could define a multivariate information between these  $N$  variables and the results of the main text would not change. In practice, however, it is very hard to perform the related numerical integration if  $N$  is large. Therefore, in the main text we show an example of two interacting units that interact through the matrix element  $\tilde{A}_{12} = 2$ . The mutual information of this model receives a distinct (and constant) contribution from the interaction matrix and from the modulation induced by  $\mathcal{D}^*$ . In fact, if we take  $A = \text{diag}(\gamma_1, \dots, \gamma_N)$ , i.e., we consider the extrinsic model, the only the contribution to the mutual information comes from the external modulation, whereas the addition of interactions simply shift the mutual information by a constant value at all  $\mathcal{D}^*$ .

## E. SCALING OF THE CORRELATION LENGTH

To study if the correlations of the system under study exhibit critical-like properties we determine the correlation length  $\xi$  of the system at various system's sizes. The correlation length can be defined as the average distance at which the correlations of the fluctuations around the mean crosses zero [46], and it is known to diverge at criticality in the thermodynamic limit [31].

For finite systems, however, this behavior can be demonstrated by showing that the correlation length grows with system size. Thus, we first compute for each time series their fluctuations around the mean, namely

$$\tilde{v}_i(t) = v_i(t) - \frac{\sum_{i=1}^N v_i(t)}{N} \quad (\text{S17})$$

where  $1/N \sum_{i=1}^N v_i(t)$  is the mean activity, i.e. the mean at time  $t$  computed over the  $N$  channels, and  $v_i$  is the activity at channel  $i$ . By definition the mean of the fluctuations vanishes, i.e.  $\frac{\sum_{i=1}^N \tilde{v}_i(t)}{N} = 0, \forall t$ . As said, different sizes (portions of the array) of the system are selected and, importantly, the mean activity is computed for each system size, considering the channels inside the observation window.

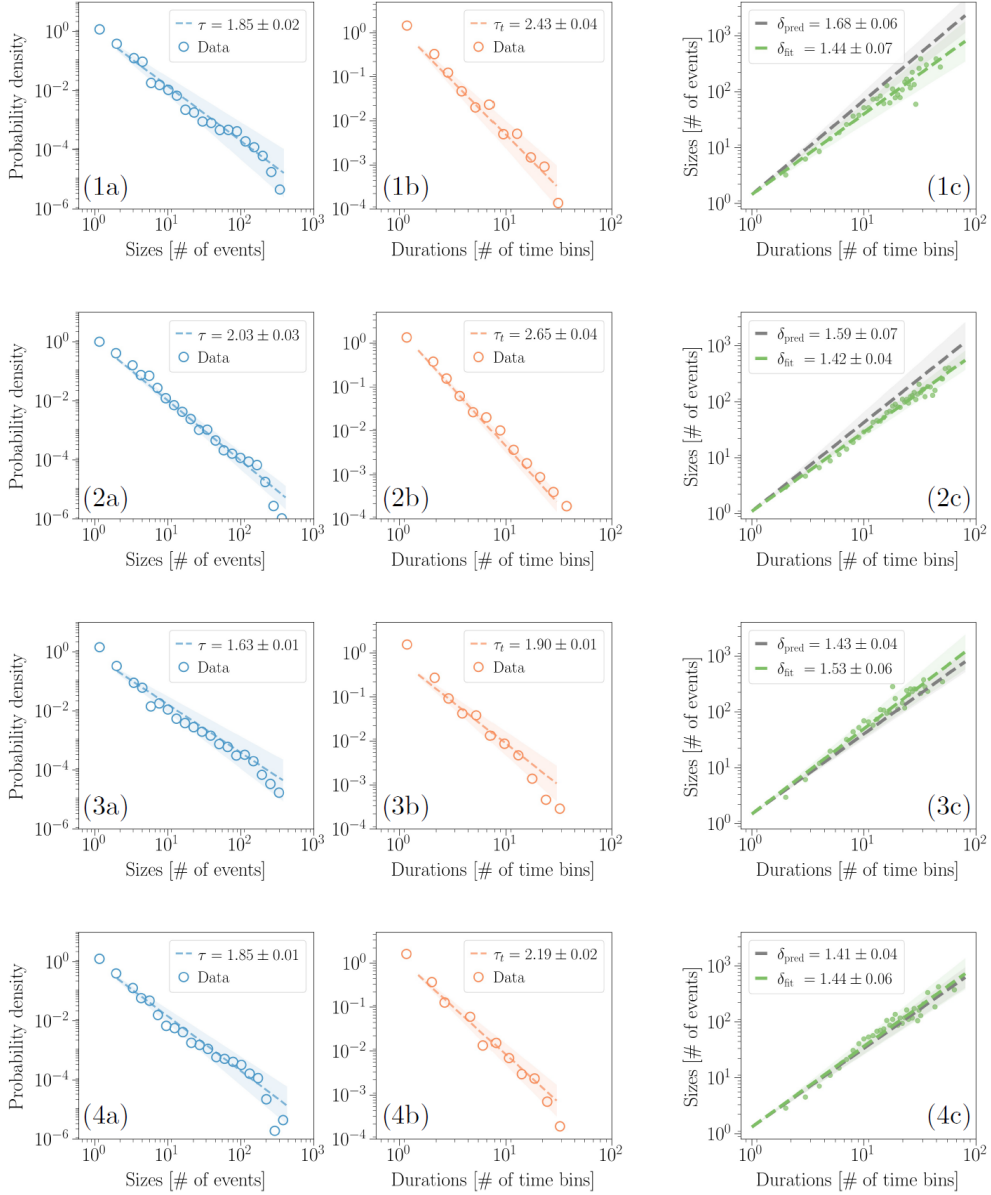


FIG. S5. Avalanche statistics in four different rats. (1a-4a) The distribution of the avalanches' sizes is consistently a power-law, with an exponent that slightly depends on the single rat. (1b-4b) The avalanche durations are once more power-law distributed in all rats with some variability in the exponents, even though the range accessible with the experimental setup only covers two decades. (1c-4c) The crackling-noise relation, however, is consistently satisfied in each rat.

In particular, since the maximum system size (corresponding to  $N$  channels) both in our experimental data and in our model is fixed, we investigate how  $\xi$  changes with system sizes corresponding to different subsamples from the multi-array probe [34]. In fact, through simulations on control models that display a critical point [65], subsampling has been shown to be practically equivalent to consider systems of different sizes. We assume that the units of our model have the same topology of our data, i.e. we assume that the units are placed as the channels in the  $55 \times 4$  array of our experimental setup.

Since in our case the array shape is rectangular, we consider the number of rows as the relevant dimension and build subsampled systems of size  $L \times 4$ , with  $L$  that decreases from the maximum of 55 channels up to 5 channels. Next, for each system's subset, we compute the average correlation function of the fluctuations between all pairs of

channels separated by a distance  $r$ ,

$$\langle C(r) \rangle = \left\langle \frac{\langle (\tilde{v}_i - \bar{v}_i)(\tilde{v}_j - \bar{v}_j) \rangle_t}{\sigma_{\tilde{v}_i} \sigma_{\tilde{v}_j}} \right\rangle_{i,j} \quad (\text{S18})$$

where  $\langle \cdot \rangle_t$  stands for the average over time,  $\langle \cdot \rangle_{i,j}$  the average over all pairs of channels separated by a distance  $r$  and

$$\begin{aligned} \bar{v}_i &= \frac{1}{T} \sum_{t=1}^T \tilde{v}_i(t) \\ \sigma_{\tilde{v}_i}^2 &= \frac{1}{T} \sum_{t=1}^T (\tilde{v}_i(t) - \bar{v}_i)^2 \end{aligned}$$

with  $T$  is the length of the time series. Then  $\xi$  is computed as the zero of the correlation function  $C(r = \xi) = 0$ . To reduce the noise effects, results were averaged across all possible sub-regions for any given size. Then the  $\xi$  are plotted against the relative system size  $L$  and the slope of the fit is obtained through a linear regression.

## F. AVALANCHES STATISTICS IN LFPS DATA

### 1. LFPS peaks detection and avalanche analysis

For the detection of LFP events, the standard deviation (SD) and the mean of the signal was computed for each channel. In order to distinguish real events from noise, a three SD threshold was chosen basing on the distribution of the signal amplitudes which significantly deviated from a Gaussian best fit above that threshold. Both negative and positive LFPs (i.e., nLFPs adn pLFPs, respectively) were considered as events in accordance with previous works [66]. Within our specific experimental settings, one reason is that across the depth of the cortex there are polarity changes of the LFP signal because of compensatory capacitive ionic currents particularly along dendrites of pyramidal cells [67]. Since in our experiments electrodes span multiple cortical layers, both nLFPs and pLFPs were found and detected. Moreover, alternatively, pLFPs can be related to activation of populations of inhibitory neurons leading to inhibitory outward postsynaptic currents, which also justifies their inclusion in the events count. For detection, each deflection was considered terminated only after it crossed the mean of the signal. After defining events of activity, the avalanche statistics are analyzed through the usual methods of the literature. In particular, the data are temporally binned, avalanches are defined as sequences of bins that present activity, and an avalanche ends once an empty bin is found - the temporal bin chosen is the average inter-event interval, as it is typically done in avalanche analysis [1]. Then, the distribution  $p(s)$  of the avalanches sizes - the number of events in each avalanche - and of the avalanche duration  $p(T)$  are computed and fitted using a corrected maximum likelihood method [43, 44]. In particular, the power law distribution is tested following the method proposed in [44, 68]. Avalanche sizes and lifetimes are fitted with discrete power laws  $p(y; \alpha) = \frac{y^{-\alpha}}{\sum_{x=x_{min}}^{x=x_{max}} x^{-\alpha}}$ . The parameter  $x_{max}$  is set to the maximum observed size or duration.  $x_{min}$  is selected as the one that minimizes the Kolmogorov-Smirnov distance (KS) between the cumulative distribution function (CDF) of the data and the CDF of the theoretical distribution fitted with the parameter that best fits the data for  $y \geq x_{min}$  [68]. To assess goodness-of-fit we compared the experimental data against 1000 surrogate datasets drawn from the best-fit power law distribution with the same number of samples as the experimental dataset. The p-value of the power-law fit was defined as the fraction of the KS statistics of the surrogates which were greater than the KS statistic for the experimental data. The data were considered power law distributed if the the p-value was greater than 0.1. We also take into account the fact that while maximum likelihood methods rely on the independence assumption, actual data often display correlations, and this may lead to false rejection of the statistical laws [44]. As the author of [44] suggest, before performing the fit and assessing p-values, we undersample the data in order to decorrelate them, by estimating the time  $\tau^*$  after which two observations (e.g., the avalanche sizes) are independent from each other, as done in [43, 44].

### 2. Avalanches statistics

Here we report the avalanches statistics from the other rats that we analyzed. The avalanches statistics is computed by considering all available the 20 trials of basal activity for each rat, that are 7.22s long. Results are reported in

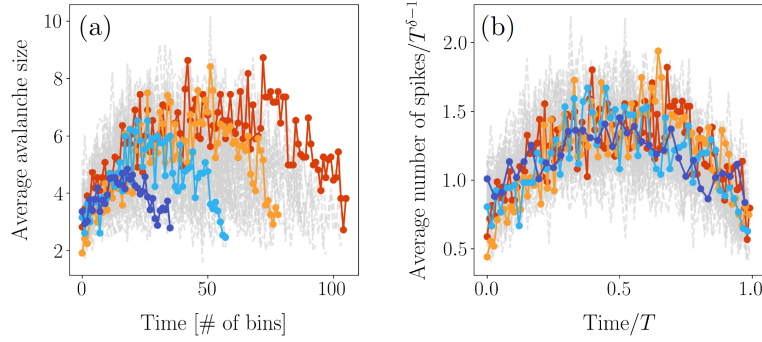


FIG. S6. Collapse of the average profile of avalanches of varying duration in the extrinsic model, for the low  $\mathcal{D}^*$  regime. (a) Profile of the avalanches before the rescaling. (b) If we rescale with an exponent  $\delta \approx 1.33$ , which is remarkably close to the one found in the main text through the crackling-noise relation, we obtain an optimal collapse onto the same scaling function.

Figure S5. Inter-rat variability is present with respect to avalanche exponents, and is expected as found in previous experiments [22, 66, 69]. Moreover, a theoretical explanation for the difference in avalanche exponents has been also recently proposed as signature of quasi-criticality [30]. However, the fundamental point is that the crackling-noise relation is always verified compatibly with the experimental errors, a feature that is usually considered a hallmark of criticality [22].

#### G. ADDITIONAL AVALANCHES STATISTICS IN THE MODEL

Another signature of criticality is the collapse of the average profile of avalanches of widely varying duration onto a single scaling function. For avalanches of duration  $T$  we can write down the average number of firing at time  $t$  as  $s(t, T) = T^{\delta-1}F(t/T)$  where  $F$  is a universal scaling function that determines the shape of the average temporal profile.  $\langle S(T) \rangle$  and  $s(t, T)$  are related by  $\langle S(T) \rangle = \int_0^T s(t, T) dt$ . At the critical point we expect that plots of  $t/T$  versus  $s(t, T)T^{1-\delta}$  for different  $T$  will collapse onto the same universal scaling function [27].

Thus, finding the exponent for which the goodness of the collapse is higher provides another way to estimate  $\delta$ . For testing the avalanche shape collapse, we used the methodology introduced in [70]. To determine the quality of the collapse, the averaged and rescaled avalanche profiles of different lifetimes  $F(t/T) = T^{1-\delta}s(t/T, T)$  are first linearly interpolated at 1000 points along the scaled duration. The variance across the different  $F(t/T)$  is calculated at each interpolated point, and the shape collapse error  $\epsilon(\delta)$  is then defined as the mean variance divided by the squared span of the avalanche shapes, where the span equals the maximum minus the minimum value of all rescaled avalanche profiles. In the presented analysis, avalanche shapes of  $T > 10$  bins with at least 10 samples were used.

The collapse has been tested on the extrinsic model in the case of low  $\mathcal{D}^*$ , and the results are plotted in Figure S6. We find that the exponent that minimizes  $\epsilon(\gamma)$  turns out to be  $\approx 1.33$ , close to the estimates of  $\delta$  found through the linear fit of average size given duration and through the prediction of the crackling-noise relation in the main text. Again, it is also close to the apparently super-universal exponent found in [22] and in [28].

#### H. THE CRACKLING NOISE RELATION AND ITS LINK WITH CRITICALITY

The so called ‘‘crackling noise’’ relation among avalanches’ distributions’ exponents [27] is usually considered a strong sign of criticality [22], however it is possible to show that it can be valid under general conditions that do not necessarily require criticality. Indeed, following arguments similar to the one proposed in [71], if we express the size  $S$  of an avalanche as a function of its duration  $T$  by assuming that  $S \sim T^\delta$ , i. e. we assume that fluctuations in the size fixed the duration can be disregarded, the following equivalence holds:

$$p(S(T)) \left| \frac{dS}{dT} \right| dT = p(T) dT$$

Then, if we assume that both  $p(S(T))$  and  $p(T)$  are described by power laws, with exponents respectively  $\tau$  and  $\tau_t$ , we see that the above equation reduces to

$$(T^\delta)^{-\tau} \delta T^{\delta-1} = T^{-\tau_t}$$

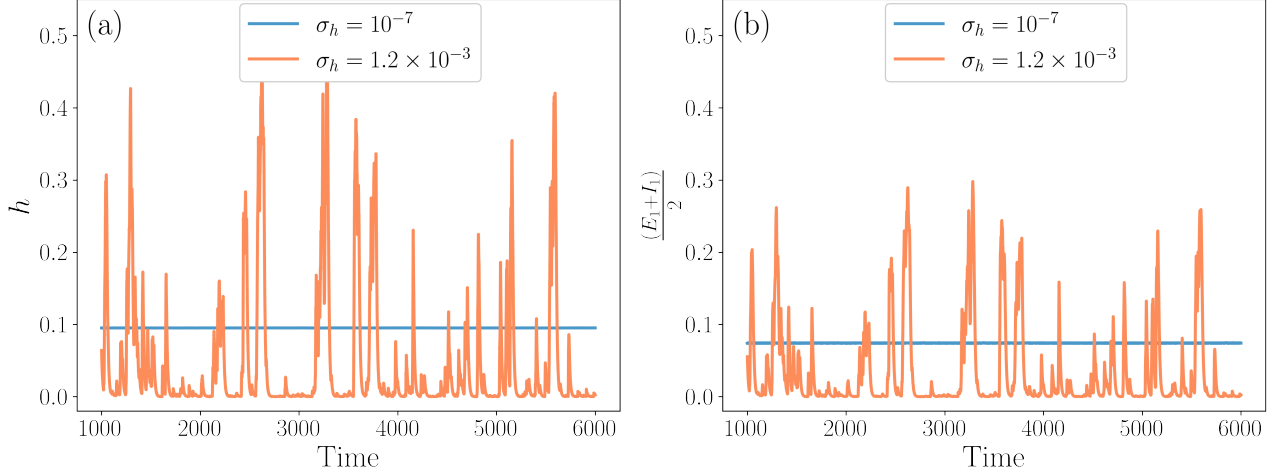


FIG. S7. (a) External input  $h = \frac{E^{(h)} + I^{(h)}}{2}$  in a balanced state ( $\omega_E^{(h)} = 50.05$  and  $\omega_I^{(h)} = 49.05$ ) with high level of noise amplitude  $\sigma^{(h)}$  (in orange), and low level of noise amplitude (in blue). When the noise level is high enough bursty behavior is present, that is reflected also on the firing rate  $\frac{E_1 + I_i}{2}$  of the units that receive  $h$  as input (Figure (b), in orange). Instead, if the noise level is low,  $h$  converges to the up state predicted by the model in the absence of noise (Fig. (a), blue), hence also the firing rate of the units (Figure (b), blue) doesn't display transient behaviors.

that leads to the relation

$$\delta = \frac{\tau_t - 1}{\tau - 1}.$$

Thus, to derive the above relation we had to assume that  $p(S)$  and  $p(T)$  are well described by power laws, and that fluctuations in the size given the duration are negligible ( $S \sim T^\delta$ ). These features are certainly proper of critical points (where moreover the exponent  $\delta$  can be expressed as a combination of other critical exponents [27]), but can be found to be valid also away from criticality, as our modeling framework shows.

## I. ALTERNATIVE MODELS

The multivariate Ornstein-Uhlenbeck (MOU) process has been previously used in the literature [50–53] to model neural activity at large scale (e.g. fMRI signals). However, it is a paradigmatic model which, albeit simple enough to allow for an analytical treatment, does not account for many biological aspects. Thus, in order to show that our results generalize to more complex situations, here we introduce a more biologically sound model that can describe the population-level neural activity measured by our LFPs data, the Wilson-Cowan model. It includes both excitatory and inhibitory synapses and non-linearities in the transfer function. We extend the framework of the extrinsic model presented in the main text, and we also provide a possible biological generative mechanism for the external time varying modulation.

The model considered is a stochastic Wilson-Cowan model [55, 56], which describes the dynamics of the activity, i.e., the density of active neurons, for the two subpopulations of excitatory (E) and inhibitory (I) neurons. Each unit  $i$ , i.e., each neural population, is now represented by a subpopulation of excitatory neurons and a subpopulation of inhibitory neurons, whose activity evolves according to the following set of stochastic equations:

$$\begin{cases} \frac{dE_i}{dt} = -\alpha E_i + (1 - E_i)f(\omega_E E_i - \omega_I I_i + h) + \sqrt{(\alpha E_i + (1 - E_i)f(\omega_E E_i - \omega_I I_i + h))}\eta_{E_i} \\ \frac{dI_i}{dt} = -\alpha I_i + (1 - I_i)f(\omega_E E_i - \omega_I I_i + h) + \sqrt{(\alpha I_i + (1 - I_i)f(\omega_E E_i - \omega_I I_i + h))}\eta_{I_i} \end{cases} \quad (\text{S19})$$

where  $\alpha$  is the rate of spontaneous activity decay,  $\omega_{E,I}$  are the synaptic efficacies,  $s = \omega_E E_i - \omega_I I_i + h$  is the averaged incoming current,  $\eta_{E,I}$  are uncorrelated Gaussian white noises, with network-size dependent amplitude  $\sigma \sim \frac{1}{\sqrt{N}}$  [55], interpreted in the Ito sense. The incoming current is modeled as the sum of all synaptic inputs plus an external input current  $h$ , filtered by a sigmoid response function

$$\begin{cases} f(s) = \tanh(s) & s \geq 0 \\ f(s) = 0 & s < 0. \end{cases} \quad (\text{S20})$$

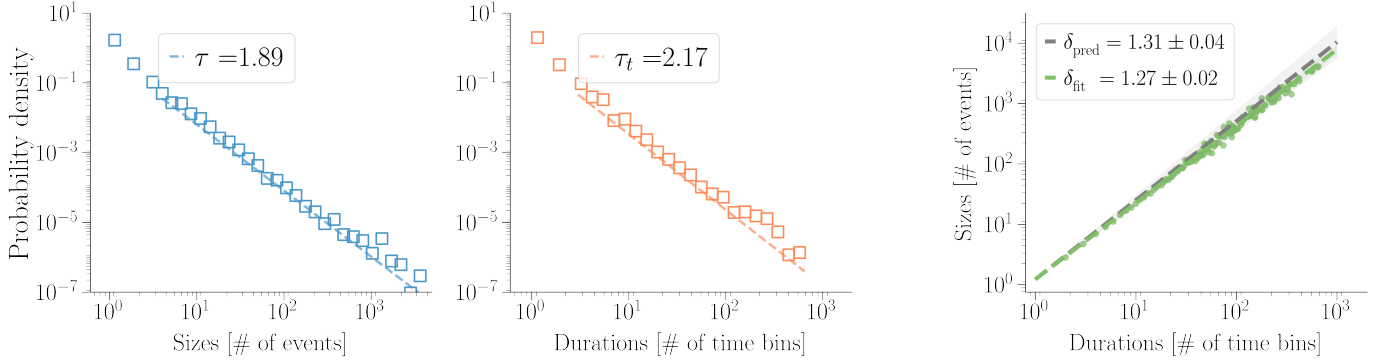


FIG. S8. Avalanches with Wilson Cowan units.

We consider a case in which the units are inhibition dominated, i.e. when  $\omega_I > \omega_E$  ( $\omega_I = 7$ ,  $\omega_E = 6.8$ ). In this situation the noise level is not going to produce significant changes in the dynamics, and the noise amplitude of  $\eta_{E_i}$ ,  $\eta_{I_i}$  is set to a low value,  $\sigma = 10^{-4} \forall i$ . Similarly, the value of  $\alpha$  is not going to affect the inhibition dominated dynamics, and it is set to  $\alpha = 1$ . For each unit, we consider the quantity  $\Sigma_i = (E_i + I_i)/2$ , that describes the firing rate of the neural population  $i$ .

As in the main text, we consider an external, time-varying input that enters the model through  $h$ . As a potential candidate for a biological realization of this external, stochastic driving, we consider the effective input that comes from other, yet unobserved, neural populations. Hence, we model  $h$  as the firing rate  $h = (E^{(h)} + I^{(h)})/2$  of another Wilson-Cowan model. In particular, we take it to be in the balanced state  $0 \ll \omega_0^{(h)} \ll \omega_{\text{sum}}^{(h)} = \omega_E^{(h)} + \omega_I^{(h)}$  and with a sufficiently high level of noise, so that the resulting firing rate spends most of the time close to the down state, while showing frequent bursts of activity [55]. Note that, since the balanced state requires that  $\omega_0 \ll \omega_S$ , it does not coincide with the “critical” state  $\omega_0 = 0$  - being balanced is not a sufficient condition and neither necessary for being critical.

We end up with a time-varying modulation

$$\frac{dh}{dt} = \frac{d}{dt} \left[ \frac{E^{(h)} + I^{(h)}}{2} \right] \quad (\text{S21})$$

that is qualitatively similar to the one considered in the main text, alternating periods of silence and bursts, but which is more realistic from a biological point of view. In particular, we choose  $\omega_E^{(h)} = 50.05$ ,  $\omega_I^{(h)} = 49.95$ ,  $h^{(h)} = 10^{-3}$ ,  $\alpha^{(h)} = 0.1$ , and, importantly,  $\sigma^{(h)}$ , the amplitude of the noise for both the excitatory and the inhibitory populations, is increased to a relatively high value,  $1.2 \times 10^{-3}$  (i.e. corresponding to a finite but still large network size), so that the up state can be destabilized by the noise. Intuitively, we are considering a case in which  $i = 1, \dots, N$  populations of neurons evolve according to the WC model in the inhibition dominated phase and are all receiving the same input by another population of neurons in a balanced state.

From each firing rate  $\Sigma_i$  we generate spike trains and analyze avalanches in the usual way, by temporal binning the events with the average inter-event interval (see the main text). Again, we find that avalanche sizes and durations are power law distributed, satisfying the crackling noise relation (Fig. S8). We note that we do not expect to find the exponents of avalanches’ sizes and durations found in [56], even though  $h$  itself is a WC model. In fact, in [56] avalanches were found by considering the excursions of  $h$  over a small threshold, in contrast to the study of spike trains carried out here. Moreover, and most importantly, the external input  $h$  that we are considering feeds the units  $i$  passing through the non linearity of  $f(s)$ , hence  $h$  and  $\Sigma_i$  do not coincide.

Thus, we have shown that the results presented in the main text, and in particular the ones of the extrinsic model, extend well beyond the paradigmatic example of a multivariate Ornstein-Uhlenbeck process with a shared external input. With respect to the approach presented in this section, the MOU has the significant advantage of being amenable to analytical treatments and to the inclusion of interactions reconstructed from the data. However, the WC model has a deeper biological relevance and proves that the mechanism proposed here for avalanche generation appears to be quite general. Finally, we note that  $h = (E^{(h)} + I^{(h)})/2$  is only one of the possible choices that could be considered for the external modulation. Other candidates include a simple Ornstein Uhlenbeck process, that is often used to model noisy neural activity [72] or the Brunel’s model in the Synchronous Irregular phase [73], which is known to be able to reproduce avalanching behavior [19].